3D-Reconstruction of Basal Cell Carcinoma

Patrick Scheibe[1], Ulf-Dietrich Braumann[2], Jens-Peer Kuska†, Markus Löffler[3], Jan C. Simon[4], Uwe Paasch[4], and Tino Wetzig[4]

[1] Translational Centre for Regenerative Medicine (TRM Leipzig),
Universität Leipzig, Philipp-Rosenthal-Straße 55, 04103 Leipzig
`pscheibe@trm.uni-leipzig.de`,
[2] Interdisciplinary Centre for Bioinformatics (IZBI), Universität Leipzig, Härtelstraße
16-18, 04107 Leipzig, Germany,
[3] Institute for Medical Informatics, Statistics and Epidemiology (IMISE),
Universität Leipzig, Härtelstraße 16-18, 04107 Leipzig,
[4] Department of Dermatology, Venerology and Allergology, Universität Leipzig,
Philipp-Rosenthal-Straße 23-25, 04103 Leipzig

Abstract. This work presents a complete processing-chain for a 3D-reconstruction of Basal Cell Carcinoma (BCC). BCC is the most common malignant skin cancer with a high risk of local recurrence after insufficient treatment. Therefore, we have focused on the development of an automated image-processing chain for 3D reconstruction of BCC using large histological serial sections. We introduce a novel kind of image-processing chain which is optimised for the diffuse nature of BCC.

For full-automatic delineation of the tumour within the tissue we apply a fuzzy c-means segmentation method, which does not calculate a hard segmentation decision but class membership probabilities. This moves the binary decision tumorous vs. non-tumorous to the end of the processing chain, and it ensures smooth gradients which are needed for a consistent registration.

We used a multi-grid form of the nonlinear registration introduced by Braumann and Kuska 2005 effectively suppressing registration runs into local minima (possibly caused by diffuse nature of the tumour). To register the stack of images this method is applied in a new way to reduce a global drift of the image stack while registration.

Our method was successfully applied in a proof-of-principle study for automated reconstruction followed by a quantitative growth analysis.

1 Introduction

Basal Cell Carcinoma (BCC) is the most common skin cancer worldwide in Caucasian populations [1]. It is a slow-growing epithelial malignant skin cancer, which tends to infiltrate the surrounding tissues and it is strongly associated with exposure to UV-irradiation [2]. The most common localisation (80 %) for BCC is the head and neck [3]. Lesions located in the mid-face or ear (so called H-zone) have a high risk of local recurrence after treatment [4]. BCC exists in different subtypes and a deeper understanding of the spatial shape is important when analysing patterns of invasion.

For other types of cancer, 3D-reconstruction methods have already been established successfully in the past [5, 6]. For the 3D-reconstruction of BCCs up to now only basic attempts were made to explore spatial features of tumour growth [7, 8]. The scattered structure of the BCC require an new registration strategy for the sequence of registration steps. In this paper we introduce a novel registration strategy for image slice stacks appropriate for diffuse cancer structures and present a proof-of-principle study for a new automated image processing chain for 3D-reconstruction as well as for the certain directional and angular morphometric growth analyses of BCC.

2 Methods

2.1 Image acquisition

Excised tissue blocks were routinely fixed and embedded in paraffin. To obtain the maximum information on the tumour, the volumes of interest (VOI) of the specimens were consecutively sliced in vertical direction with a thickness of 6 μm.

For routine, haematoxylin eosin (H&E) staining of all slides were subjected to automated staining using a linear stainer (Microm, Germany). Histological examination following finalisation of the processing by automated covering using standard glass cover slips was performed by an independent investigator who checked whether or not the lesions were completely excised.

Whole histological specimens with verified tumour tissue were subjected for scanning with an automated system for digital pathology (MIRAX MIDI, Carl Zeiss, Germany). For the reconstruction a downscaled version of colour-images was used, each with a resolution of 1000×400 pixels and a nominal pixel size of $15 \, \mu m \times 15 \, \mu m$.

Not all images are appropriate for the reconstruction due to heavy folds in the slices which sometimes appear in the process of slicing and staining. The images of these slices were not used and finally filled with their neighbouring slice.

2.2 Preprocessing and Segmentation

The first step of the processing chain is a rigid registration. It roughly co-registers consecutive image pairs by applying a combination of translation, rotation and scaling. For a reference image $R(\boldsymbol{x})$ and a deformable template image $T(\boldsymbol{x})$ this registration step tries to find the optimal parameters of a transformation $\boldsymbol{u}(\boldsymbol{x}) : \Omega \to \Omega$ with $\boldsymbol{x} = (x_1, x_2)^\top \in \Omega \subset \mathbb{R}^2$. In the case of a rigid registration the transformation is given by

$$\boldsymbol{u}(\boldsymbol{x}) = \boldsymbol{A}\boldsymbol{x} + \boldsymbol{b}_r \quad \text{with} \quad \boldsymbol{A} = \begin{pmatrix} s_r & 0 \\ 0 & s_r \end{pmatrix} \begin{pmatrix} \cos \alpha_r & -\sin \alpha_r \\ \sin \alpha_r & \cos \alpha_r \end{pmatrix} \tag{1}$$

and the optimal parameters are found when a certain distance measure $\mathcal{D}$ between the images $R(\boldsymbol{x})$ and $T(\boldsymbol{u}(\boldsymbol{x}))$ is minimised, which is here the sum of

squared differences between the images

$$\mathcal{D}(\boldsymbol{u}) = \frac{1}{2} \int_{\varOmega} \left[T(\boldsymbol{x} - \boldsymbol{u}(\boldsymbol{x})) - R(\boldsymbol{x}) \right]^2 d\boldsymbol{x}. \tag{2}$$

Throughout this work we tried to be consistent with the notation-style of Modersitzki [9]. This registration step is fundamental to the success of the second non-linear registration which follows after the segmentation. This is caused by the fact that it is more likely that the following non-linear registration succeeds when the images are already near the solution and the registration has to compensate small local differences only.

The effect of the rigid registration can be observed in fig. 1(a). The top image shows an unregistered set of slides, whereas the bottom image clearly documents that after registration the slides fit quite well onto another.

All images are now filtered through a total variation (TV) filter suggested by Chan et al. [10] to reduce noise in images while preserving structure edges. This step is necessary since the segmentation preferably needs images of smooth tissue areas with clear edges to succeed. Other edge preserving denoising operators like median filters or non-linear diffusion filters preserve the edges not so well (median filter) or need more parameter (non-linear diffusion filter). The only parameter the TV filter requires is the estimated standard deviation of the noise whereas this feature is easy to be estimated from background parts of a typical image.

2.3 Tumour Segmentation

The smoothed images are the basis for the fuzzy c-means segmentation [11, 12]. The reasons for choosing the fuzzy c-means algorithm are threefold: This algorithm does not make a sharp decision which area in the image belongs to which class in the segmentation result but rather provides a probability of the membership. This is crucial since the H&E-staining produces violet images with different saturations for tumorous and non-tumorous parts. These parts sometimes overlap in colour-space and at this stage of the reconstruction a sharp decision for a pixel which is given by other segmentation methods is not adequate. Therefore, segmentations like c-means or mean shift cannot be used.

The second reason is that the colour saturation of the slices changes due to instabilities in the staining procedure. Therefore, an overall (3D) segmentation of the colour space is not possible, because the same colour can correspond to different tissue types in different slices due to different slice thickness and exposure time to the staining chemicals. The fuzzy c-means segmentation does solve this problem by an adaptation of already calculated segmentation-class-distributions and therefore provides constantly good tissue segmentation results throughout the whole image stack.

The third reason for the choice of the fuzzy c-means method is that segmentation results are approximated memberships of the pixels to colour classes. Since these membership probabilities are represented as grey-levels and not as binary-values they provide smooth gradients which are important for the non-linear image registration.

As mentioned before, the used fuzzy c-means method is able adapt a given set of colour-centres as starting point for a new image and calculate a segmentation on this basis. Therefore, in the segmentation-process of the complete image stack we had to verify only one segmentation-result and for the rest of the images it was not necessary to adjust any parameters.

In fig. 1(b) the main steps of the image processing chain are depicted, in particular both the smoothing and segmentation step. The small layer of the epidermis and the adjacent tumour tissue are too close together in colour-space and are not separable by the segmentation. However, it was possible to extract this layer automatically by taking the mask of the background of each slide and enlarge it by the size of the epidermis. This step which is depicted in fig. 1(c) completes the extraction of the tumour.
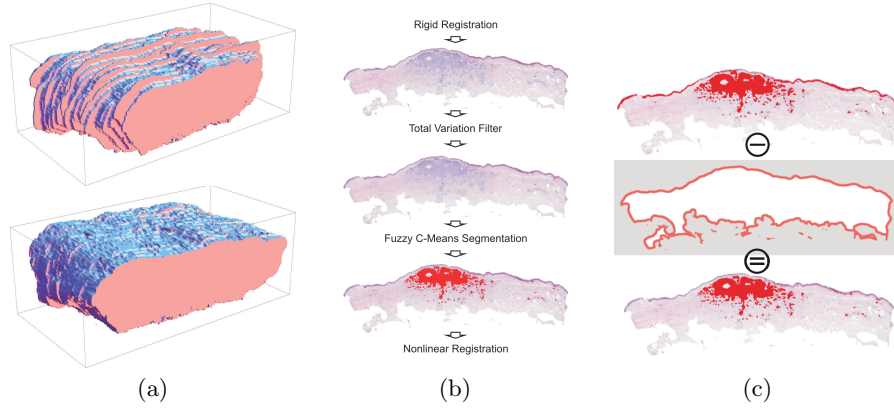

Fig. 1. (a) Shape of an unregistered (top) and the rigid registered (bottom) image-stack. (b) The flowchart shows the main steps of the tumour segmentation. To demonstrate the edge-preserving behaviour of the Total Variation Filter we took extreme filter parameters for this example. Those are not necessary in the real process chain. (c) The automatic extraction of the epidermis is possible with the grown background-mask of the segmentation. This mask is is grown by the size of the epidermis and is then used to mask out the regions in the segmentation result.

2.4 Reconstruction

At this point it is necessary to re-align local differences in tumorous parts of consecutive slides. During preparation, inevitable deformations occur, which need to get compensated. For this purpose a non-linear registration step was applied which was working on intensity images resulting from a combination of the approximate class membership for the cancer class obtained from the fuzzy c-means segmentation and a low-level intensity image of the slide itself. Primarily we are

interested in a mapping of the tumour regions, but to get a consistent result, the usage of the slide intensity in regions without tumour is essential.

As already mentioned in the segmentation section the registration of the approximate class membership from the segmentation procedure provides smoother gradients which means less local gradients for the non-linear registration procedure than one would obtain by hard segmented images.

The non-linear registration after the rigid registration step is necessary since this method can stretch and bend parts of the image to bring the tumour tissue of adjacent slides onto another. The method of choice at this point bases on the optical flow and was firstly mentioned by Amit [13] and Modersitzki [9] and later extensively used by Braumann and Kuska [5, 14].

In the process of registration the required displacement field $\boldsymbol{u}(\boldsymbol{x}) : \Omega \rightarrow \Omega$ is found by minimising a joint registration criterion

$$\min_{\boldsymbol{u}} \left(\mathcal{D}(\boldsymbol{u}) + \alpha \mathcal{S}(\boldsymbol{u}) \right) \tag{3}$$

consisting of the already mentioned distance measure

$$\mathcal{D}(\boldsymbol{u}) = \frac{1}{2} \int_{\Omega} \left[T(\boldsymbol{x} - \boldsymbol{u}(\boldsymbol{x})) - R(\boldsymbol{x}) \right]^2 d\boldsymbol{x} \tag{4}$$

and smoothing term

$$\mathcal{S}(\boldsymbol{u}) = \frac{1}{2} \sum_{i=1}^{2} \int_{\Omega} (\Delta u_i)^2 d\boldsymbol{x}. \tag{5}$$

Using the calculus of variations, the solution for equation (3) will require to solve a system of 4th order partial differential equations. Different approaches are possible but in this work we used the multi-grid implementation which is described in more detail in [5].

Likewise, we registered the whole set of images so that every slide is co-registered onto its predecessor. Usually the image-stack is processed in a single run and one (forward) direction. This procedure excels the chosen direction over the opposite one which is adequate for relatively solid structures and tissue types. The diffuse nature of the BCC and the fact that the skin is not completely surrounded by stabilising tissue require a more symmetrical alignment of the slices which is in this work ensured by not processing the images of the stack in one registration run. Instead, we registered at first each image pair-wise with its neighbour starting at the first image and processing in forward direction through the stack breaking up the registration before it converges. Thereafter we proceed backwards through the image stack with the same approach and repeated the whole procedure three times.

2.5 Visualisation

After this last step the reconstruction chain is finished and the result is a 3D-tumour-density field which is the basis for further morphological analysis and 3D

visualisation. In the case of this work we calculated an iso-surface of the largest connected component of the tumour. For that purpose a 3D total variation filter on the tumour density was used in order to smooth the data for visualisation.

After that, a volume labelling algorithm was utilised to mark connected parts with an ID and calculate their volume. With position and volume of all objects we could verify that the biggest component was the main tumour-object (see fig. 3).

2.6   Quantification

To characterise the tumour we want to determine the dependency of the distance distribution with respect to different angles and radii in spherical and cylindrical coordinates, respectively. For both approaches we have chosen the point of origin to be the centre of masses of the tumour projected onto the topmost horizontal plane of the bounding-box (the xy-plane in our coordinate system). This centre is depicted in figure 2(a) as point of intersection of the radii and in figure 2(c) as centre of the concentric circles. It can be obtained by

$$\boldsymbol{m} = P_{xy}\left(\frac{1}{N}\sum_{i=1}^{N}\boldsymbol{x}_i\right),\tag{6}$$

where $\boldsymbol{x}_i$ are all positions of tumour in the data set and P_{xy} is the projection onto the xy-plane.

In this work the primary focus is put on the invasion of BCC in the surrounding tissue whereas the lateral propagation *direction* is not in the main focus. Therefore, we are in the first rank rather interested in the dependency on the polar angle as depicted in figure 2(a). With

$$\boldsymbol{t}_{\mathrm{sp}}(\boldsymbol{x}) = \left(\arctan\left(\frac{\sqrt{x_1^2 + x_2^2}}{x_3}\right)\ ,\ \sqrt{x_1^2 + x_2^2 + x_3^2}\right)^{\top}\tag{7}$$

we can transform all positions $\boldsymbol{x}_i$ of tumour in the data set by calculating

$$\boldsymbol{r}_i = \boldsymbol{t}_{\mathrm{sp}}(\boldsymbol{m} - \boldsymbol{x}_i).\tag{8}$$

This list is now quantised into different angular intervals. Note that the angles in this list are all in the main interval $[0, \pi/2]$ since (i) in the hemisphere above the centre $\boldsymbol{m}$ (a region outside the skin) there is no tumour and (ii) corresponding radii left and right of $\boldsymbol{m}$ in figure 2(a) represent the same polar angles.

All collected radii of an angular interval can be treated as realisation of a Γ-distributed random variable, since the Γ-distribution is the only distribution going along with the power of the random variable. The probability density function of a gamma distribution is given by

$$f_{\Gamma}(r; k, \Theta) = r^{k-1}\frac{\Theta^{-k}\exp(-r/\Theta)}{\Gamma(k)}\quad\text{where}\quad \Gamma(k) = \int_0^{\infty} t^{k-1}\exp(-t)\mathrm{d}t\tag{9}$$
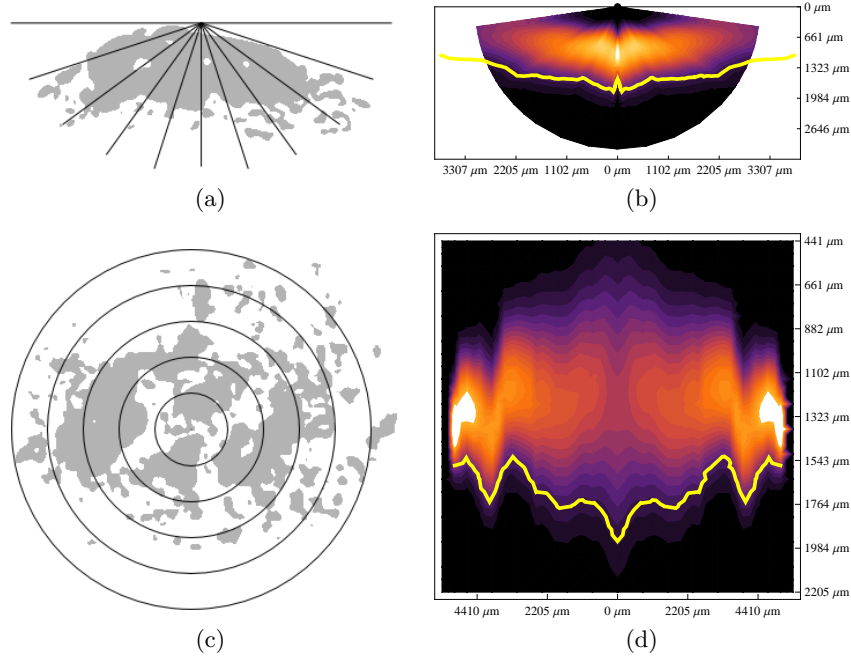
Fig. 2. While (a) is a sectional view of a virtual cutting plane orthogonal to the skin surface, where the lines indicate different polar angles, (c) shows a plane parallel to the skin with different radii. The different angles and radii are used in the density plots (b) and (d) of probability distributions obtained by the quantification methods. The origin of the coordinate system is in both cases the reference point $\boldsymbol{m}$. The yellow lines denote the $P(X \leq 0.95)$ border. (b) is a plot of the angular distribution where angles are transformed back to Cartesian coordinates and (d) is a plot of the depth distribution.

with the parameters (k, Θ). In order to estimate values for these parameters we used an iterative maximum likelihood estimation (MLE) scheme [15]. The parameters found by the MLE algorithm are the basis for distribution analysis as is detailed in the following section.

Going beyond the angular analysis, more information can be extracted using a method reflecting the depth distribution of BCC. We step in after the calculation of the reference point $\boldsymbol{m}$ (eq. 6), but now we are interested in the probability of the tumour depth at a given distance from $\boldsymbol{m}$. Therefore we use cylindrical coordinates and analyse the depth distribution of different range intervals as basically depicted in figure 2(c).

In this approach all positions $\boldsymbol{x}_i$ of tumour are transformed by

$$\boldsymbol{r}_i = \boldsymbol{t}_{\mathrm{cy}}(\boldsymbol{m} - \boldsymbol{x}_i) \quad \text{where} \quad \boldsymbol{t}_{\mathrm{cy}}(\boldsymbol{x}) = \left(\sqrt{x_1^2 + x_2^2} \, , \ x_3 \right) \tag{10}$$

which are the first and the last component of cylindrical coordinates. The rest of the approach is similar to the first method besides the fact that the estimated tumour depth distribution is normal distributed.

3 Results

The present data-set is based on a serial section of a complete BCC which consists of 193 slices. From this data-set 43 slices had to be excluded due to folds or artifacts. The specimen has a volume of 80 mm^3 and contains a segmented tumour of about 2.6 mm^3.

The 3D-iso-surface plot depicts the tumour component (fig. 3). To enhance illustration it was artificially enlarged and embedded behind the surface of the tissue specimen. Since we only have visualised the largest component, we had to verify that all small segments previously masked out were indeed false positives. i.e., 3D-coordinates of them were taken, thereafter the dermatopathologist classified all segments to be false positive.

As already mentioned, epidermis and tumour are not well separable in H&E-stained slices using the applied staining-based segmentation method. Another source for false-positive segmentation are hair follicles. While the epidermis can be identified by its closeness to the tissue boundary and therefore can be masked out by the above mentioned steps, hair follicles are identifiable due to their characteristics in the final reconstruction.

A hair follicle is an epidermal sheath that surrounds the hair. Sebaceous glands are usually attached to the side of a follicle. Their oily secretion enters the follicle and follows it to the surface. The hair grows from the bulb, swollen lower end of the follicle. The bulb is invested with blood vessels and nerves. Due to these typical histological characteristics they can easily identified and extracted from the volume.

A new method for the non-linear registration of the slice stack in several runs with different directions in the slice stack has been introduced. The new method has shown to work well with diffuse cancer structures like the BCC.

4 Discussion

This work has successfully given a proof-of-principle for an image processing chain for a 3D-reconstruction of BCC. The starting point was an H&E stained large serial histological section from paraffin embedded specimen.

Unlike established microscopic imaging techniques such as confocal laser scanning microscopy (CLSM), or the bread leaf sectioning technique as applied in histopathological routine, in Mohs micro-graphic surgery [4] used by Braun [7], our new approach relying on histological serial sections allows for (i) a complete tissue volume reconstruction, (ii) visualisation of the whole tumour including surrounding tissue and (iii) quantification of statistical properties.

CLSM, however, cannot provide a sufficient penetration depth of several millimetres. The bread leaf sectioning obviously takes far too less (non-adjacent!)
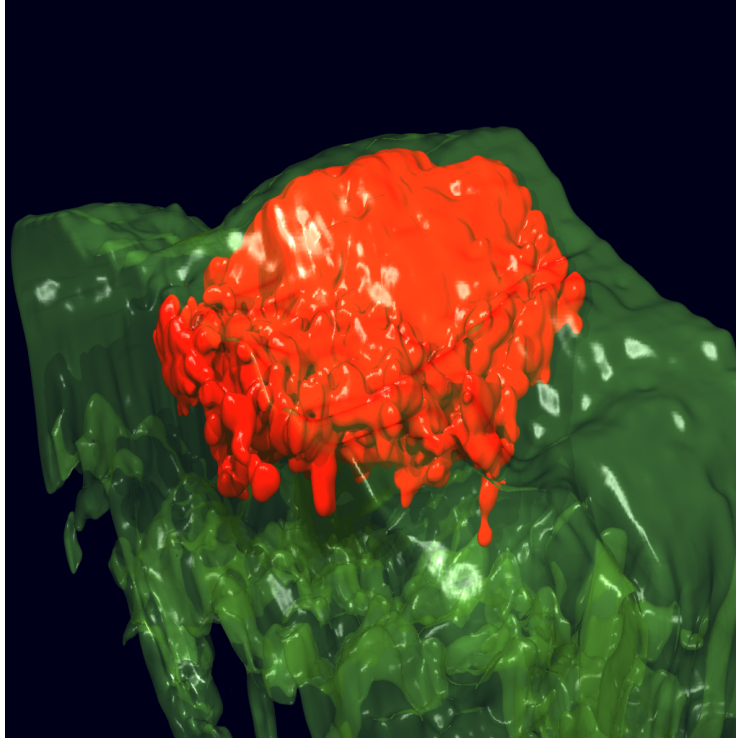
Fig. 3. An iso-surface plot of the reconstructed BCC (red) embedded behind the surface of the tissue specimen (green).

sections for registration-based reconstructions. Mohs surgery relies on cryosections and uses horizontal sectioning, hence the method, besides the flat-bed scanning and manual tumour delineation as done by Braun [7], will not provide sufficient preparation quality as can be obtained using paraffin embedding and vertical sectioning, the latter preserving the epidermis.

Instead, our approach utilises virtual microscopy for image capture, as well as state-of-the-art image processing methods for the successive image series registration in order to re-establish a 3D histological data-set. We therefore applied a sophisticated non-linear image registration algorithm (optical flow method) in order to ensure that unavoidable distortions as occur during manual sectioning and further slice preparation (staining-induced partial shrinking) can be compensated within the image data.

Further, the staining-based automatic tumour segmentation (fuzzy c-means method), even though ending up with a few false-positives as e.g. hair follicles, is essential to treat data-sets consisting of hundreds of images per series. To replace the remaining minimum of manual interaction to sort out respective false positive regions would require knowledge-based approaches to get eliminated in future, but this was not the focus of this work.

However, since segmentation quality is crucial for our method, in preliminary work we have evaluated the reliability of tumour segmentation in H&E stained single sections of 10 randomly selected BCCs of different sub-types. After careful inspection of the results by the dermatopathologist it turned out that the segmentation is appropriate to detect all tumorous parts. The sources of false positive segmented tissue remained restricted to parts of epidermis, sebaceous gland, and hair follicles.

The present proof-of-principle study demonstrates the first feasible approach to elucidate the 3D tumour growth of a complete BCC in microscopic resolution. The volume data obtained by the presented method is considered highly appropriate for further phenotypical investigations in order to morphometrically describe tumour growth.

One such detail of interest is e.g. how an objective description of the spatial tumour distribution can be obtained. For this purpose it is possible to determine the dependence of the distance distribution with respect to different polar angles in spherical coordinates. Through such a characterisation distances from the centre of the BCC can be calculated which have a certain probability that none of the tumorous tissue infiltrates into deeper regions of the skin.

For this approach we chose the origin $\boldsymbol{m}$ of the spherical coordinate system to be the centre of masses of the tumour projected onto the topmost horizontal plane of the bounding-box. This choice is motivated by the idea that it is possible for the surgeon to identify this centre on the skin. After the transformation in spherical coordinates the data-set is quantised into different angular intervals. Note that these angles are all in the main interval $[0, \pi/2]$ since (i) on the hemisphere above $\boldsymbol{m}$ there is no tumour and (ii) corresponding radii left and right of $\boldsymbol{m}$ represent the same polar angles, since the azimuth dependence is not taken into account.

The next step is to treat all collected radii of an angular interval as realisation of a Γ-distributed random variable, since the Γ-distribution is the only distribution going along with the power of the random variable. In order to estimate values for these parameters we used an iterative maximum likelihood estimation (MLE) scheme [15]. The parameters found by the MLE algorithm are the base for distribution visualisation given in fig. 2(b). Since the dependence on the azimuth was not taken into account, the visualisation is symmetric to the centre. The colour ranges from black to white and denotes the probability interval $[0, 0.03]$. The yellow line is the P_{95} border which states 95% of the tumour is below this radius.

With methods like the presented one, another future application is the validation of new non-invasive high-resolution skin imaging techniques. In general, for detailed objective insights into shape, structure and growth patterns further investigations in 3D-quantification techniques for BCC are required as next step after a 3D-reconstruction.

References

1. Raasch, B.A., Buettner, P.G., Garbe, C.: Basal cell carcinoma: histological classification and body-site distribution. Br J Dermatol **155**(2) (Aug 2006) 401–407
2. Rigel, D.S.: Cutaneous ultraviolet exposure and its relationship to the development of skin cancer. J Am Acad Dermatol **58**(5 Suppl 2) (May 2008) S129–S132
3. Woerle, B., Heckmann, M., Konz, B.: Micrographic surgery of basal cell carcinomas of the head. Recent Results Cancer Res **160** (2002) 219–224
4. Swanson, N.A.: Mohs surgery. technique, indications, applications, and the future. Arch Dermatol **119**(9) (Sep 1983) 761–773
5. Braumann, U.D., Kuska, J.P., Einenkel, J., Horn, L.C., Löffler, M., Höckel, M.: Three-dimensional reconstruction and quantification of cervical carcinoma invasion fronts from histological serial sections. IEEE Transactions on Medical Imaging **24**(10) (October 2005) 1286–1307 http://dx.doi.org/10.1109/TMI.2005.855437.
6. Braumann, U.D., Scherf, N., Einenkel, J., Horn, L.C., Wentzensen, N., Loeffler, M., Kuska, J.P.: Large histological serial sections for computational tissue volume reconstruction. Methods Inf Med **46**(5) (2007) 614–622
7. Braun, R., Klumb, F., Bondon, D., Salomon, D., Skaria, A., Adatto, M., French, L., Saurat, J., Vallee, J.: Three-Dimensional Reconstruction of Basal Cell Carcinomas. Derma Surg **31**(5) (2005) 562–569
8. Matsumura, T., Sato-Matsumura, K.C., Yokota, T., Kobayashi, H., Nagashima, K., Ohkawara, A.: Three-dimensional reconstruction in dermatopathology–a personal computer-based system. J Cutan Pathol **26**(4) (Apr 1999) 197–200
9. Modersitzki, J.: Numerical Methods for Image Registration (Numerical Mathematics and Scientific Computation). Oxford University Press, USA (2004)
10. Chan, T., Osher, S., Shen, J.: The digital tv filter and non-linear denoising (2001)
11. Bezdek, J.: Pattern Recognition with Fuzzy Objective Function algorithms. Plenum, New York (1981)
12. Dunn, J.C.: A fuzzy relative of the ISODATA process and its use in detecting compact well-separated clusters. Journal of Cybernetics **3** (1973) 32–57
13. Amit, Y.: A nonlinear variational problem for image matching. SIAM Journal on Scientific Computing **15**(1) (January 1994) 207–224
14. Braumann, U.D., Kuska, J.P.: Influence of the boundary conditions on the result of non-linear image registration. In: Proceedings of the IEEE International Conference on Image Processing, IEEE Signal Processing Society (September 2005) I-1129–I-1132
15. Choi, S., Wette, R.: Maximum likelihood estimation of the parameters of the gamma distribution and their bias. Technometrics **11**(4) (1969) 683–690